Yiting Xie ; Anthony P. Reeves; Single 3D cell segmentation from optical CT microscope images. Proc. SPIE 9034, Medical Imaging 2014: Image Processing, 90343B (March 21, 2014);

doi:10.1117/12.2043852.

© (2014) COPYRIGHT Society of Photo-Optical Instrumentation Engineers (SPIE). Downloading of the paper is permitted for personal use only. Systematic or multiple reproduction, duplication of any material in this paper for a fee or for commercial purposes, or modification of the content of the paper are prohibited.

Single 3D cell segmentation from optical CT microscope images

Yiting Xie and Anthony P. Reeves

School of Electrical and Computer Engineering, Cornell University, Ithaca, NY, USA

ABSTRACT

The automated segmentation of the nucleus and cytoplasm regions in 3D optical CT microscope images has been achieved with two methods, a global threshold gradient based approach and a graph-cut approach. For the first method, the first two peaks of a gradient figure of merit curve are selected as the thresholds for cytoplasm and nucleus segmentation. The second method applies a graph-cut segmentation twice: the first identifies the nucleus region and the second identifies the cytoplasm region. Image segmentation of single cells is important for automated disease diagnostic systems.

The segmentation methods were evaluated with 200 3D images consisting of 40 samples of 5 different cell types. The cell types consisted of columnar, macrophage, metaplastic and squamous human cells and cultured A549 cancer cells. The segmented cells were compared with both 2D and 3D reference images and the quality of segmentation was determined by the Dice Similarity Coefficient (DSC).

In general, the graph-cut method had a superior performance to the gradient-based method. The graph-cut method achieved an average DSC of 86% and 72% for nucleus and cytoplasm segmentations respectively for the 2D reference images and 83% and 75% for the 3D reference images. The gradient method achieved an average DSC of 72% and 51% for nucleus and cytoplasm segmentation for the 2D reference images and 71% and 51% for the 3D reference images. The DSC of cytoplasm segmentation was significantly lower than for the nucleus since the cytoplasm was not differentiated as well by image intensity from the background.

Keywords: single cell segmentation, optical CT, graph-cut

1. INTRODUCTION

Three-dimensional analysis of a single cell is made possible by the technique of optical projection-based 3D computed tomography [1]. The basic organization of this device is shown in Figure 1. The 3D cell imaging technique comprises of the following steps: (1) fix a cell and perform absorption-based staining; (2) suspend the cell in an optical-gel that is injected into a capillary tube (50μm inner diameter); (3) take optical projection images from 500 different perspectives by rotating the specimen by 360°; (4) perform tomographic reconstruction using a filtered back-projection method which is standard technique for X-ray CT. In the reconstruction, the 3D voxel is cubic with a 0.35μm spatial resolution. Prepared stained cells within an optical gel of constant refractive index are inserted one at a time into a capillary tub. Once the cell is located at the imaging stage the tube is rotated by 360° at an increment of 0.72° in 500 steps. For each of these step an in focus projection image of the cell is acquired by recording a set of images at successive focal distances through the target and then combining them together. The range of focal plane scanning is based on the specimen, which can be as small as a single nucleus.

The novel Cell-CT imaging technique enables the 3D quantitative analysis of cells. Compared to 2D images, 3D cell image features are not affected by cell orientations and provide more precise and useful measurement information [1-3].

Medical Imaging 2014: Image Processing, edited by Sebastien Ourselin, Martin A. Styner, Proc. of SPIE Vol. 9034, 90343B · © 2014 SPIE
CCC code: 1605-7422/14/$18 · doi: 10.1117/12.2043852

Downloaded From: http://proceedings.spiedigitallibrary.org/ on 08/10/2016 Terms of Use: http://spiedigitallibrary.org/ss/termsofuse.aspx

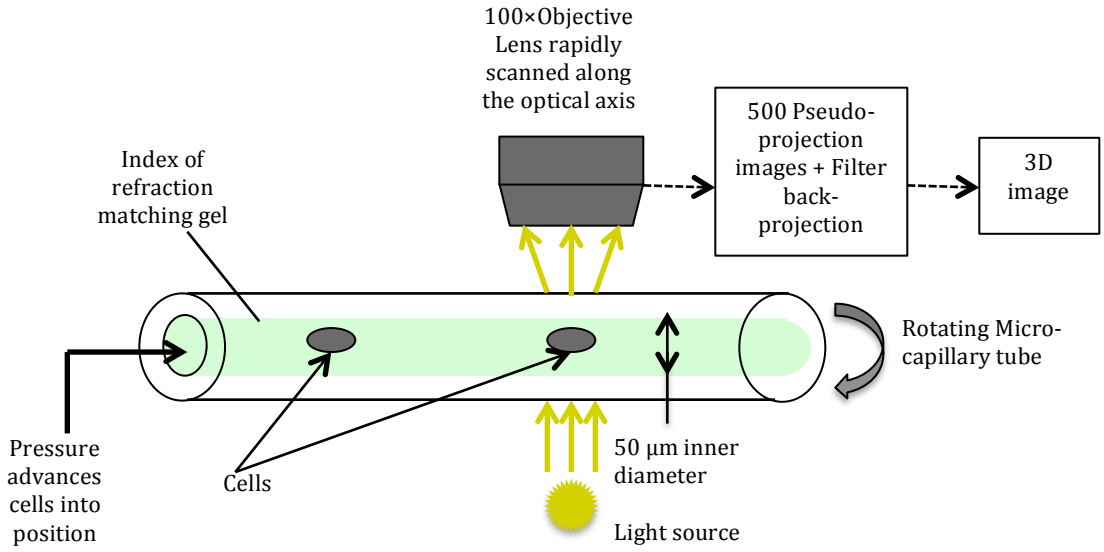

Figure 1. Illustration of the operation of the optical projection Cell-CT system [4].

This paper presents fully automated single cell segmentation algorithms for 3D images. Five types of cells A549 lung cancer (AF), columnar (CO), macrophage (MA), metaplastic (ME), and squamous (SQ) were used for segmentation evaluation. In previous work, Meyer et al [4] compared 2D and 3D classification of human lung adenocarcinoma cells (A549, cancer cells) against normal human airway epithelial cells (SAEC, non-cancer cells) based on nucleus features such as size, shape and intensity distribution. The nucleus segmentation in [4] was performed by applying a threshold, which was chosen based on the peak value of the cell intensity histogram. This method might not perform very well on cytoplasm segmentation since there might be no obvious peak to separate cytoplasm region from image background. Reeves et al. [3] measured the 2D and 3D nuclear cytoplasmic ratio (NC ratio) of the same 5 types of cells (AF, CO, MA, ME and SQ). The nucleus and cytoplasm regions were extracted using a threshold value obtained from ground truth markings; fully automated segmentation was not performed. Two different automated segmentation algorithms have been developed and evaluated: the first one is based on gradient information at different thresholds and the second one is based on sequential graph-cut applications.

2. METHODS

A 3D optical CT cell image can be modeled as an object with three distinct intensity values: a low-intensity background, an intermediate intensity cytoplasm and a much higher intensity nucleus. Thus going from the background to the center of the cell, two rapid intensity transitions are expected: once for the background-cytoplasm boundary and once for the cytoplasm-nucleus boundary.

The first algorithm, the gradient approach, is based on the concept that pixel intensities in 3D cell image should map well to optical absorption values as they do with convectional X-ray CT. For this condition a single global threshold should be sufficient for a good segmentation. Further, the boundary pixels of the regions selected by the optimal threshold should all have a high gradient value (since they are in the transition region between outside and within the segmented object). In the gradient algorithm a gradient figure of merit is computed for each possible threshold value. This figure-of-merit is the average gradient level for the boundary pixels selected by the threshold. It should have a maximum value when the threshold selects pixels in the transition between two regions of different intensities.

Downloaded From: http://proceedings.spiedigitallibrary.org/ on 08/10/2016 Terms of Use: http://spiedigitallibrary.org/ss/termsofuse.aspx

A figure of merit curve containing gradient information is computed based on the center axial slice using the following algorithm (also see figure 2).

The Gradient segmentation algorithm

(1) Compute a gradient image *G;* for this algorithm the Deriche gradient operator was used [6];
(2) Compute a gradient figure of merit value for each possible image threshold value. That is computing the mean gradient value selected by the border pixels.
(3) Plot the gradient figure of merit for all possible threshold values; the first two peaks of this graph correspond to the global thresholds for background/cytoplasm and for cytoplasm/nucleus segmentation respectively.

For gradient-based method, the image intensity of the cell was from 0 to 255. In order for the algorithm to be robust to noise, the following post-processing was performed:

(1) The figure of merit curve was smoothed to avoid selecting a false peak due to noise. Smoothing was accomplished by mean filtering each plot point with a window of size $2k+1$. For this algorithm setting k to 3 was found to be sufficient.
(2) A constraint on the minimum distance between two peaks was set to be 30 to eliminate adjacent peaks caused by image noise.
(3) After thresholding, for both nucleus and cytoplasm region, only the largest connected component was selected to reject other objects in the image that were not part of the cell.

This algorithm is illustrated by an example shown in Figure 2. In this case the algorithm is applied to a single central image slice of a 3D cell image. It shows the original intensity image, the gradient image and the final segmentation result with the nucleus in red and the cytoplasm in green. Figure 3 shows the gradient figure of merit plot for this image. The two clear peaks indicate the segmentation threshold values.

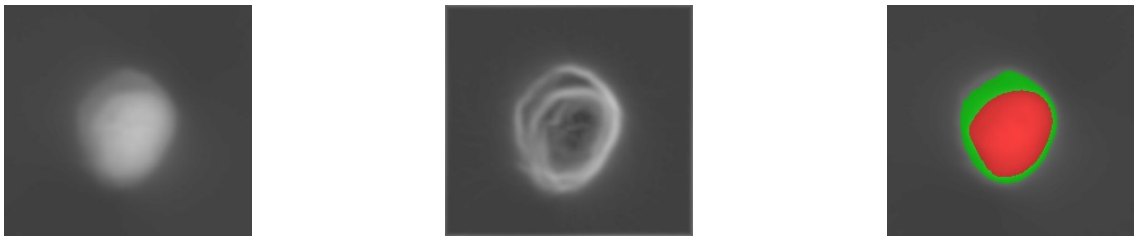

Intensity Image Gradient Image *G* Segmentation Result

Figure 2. Gradient segmentation method. From left to right: the center slice of a cell image, its gradient image and segmentation result (red for nucleus and green for cytoplasm region).

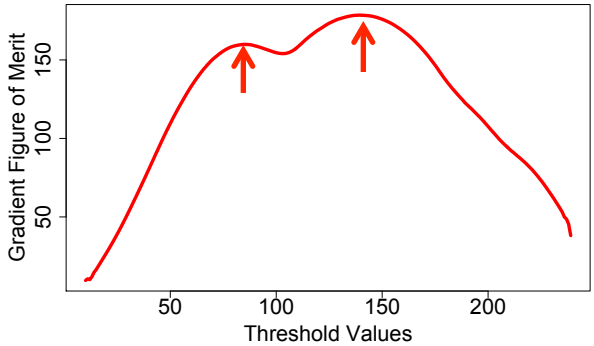

Figure 3. Gradient figure of merit. The two red arrows indicate the two peaks used as segmentation threshold values.

While the gradient algorithm provided excellent results for many cell images, for many other images the results were very poor especially for the cancer cells that had highly irregular nuclei with very large intensity variations.

Downloaded From: http://proceedings.spiedigitallibrary.org/ on 08/10/2016 Terms of Use: http://spiedigitallibrary.org/ss/termsofuse.aspx

Further, for all image slices there was some intensity variation throughout the 3D image, which meant that a good segmentation result could not be obtained by any single global threshold. To allow for some local variation in the threshold value a graph-cut algorithm was considered.

The graph-cut convex hull algorithm

The graph-cut algorithm presented by Boykov et al.[5] formulates segmentation as a binary labeling problem: a pixel is either inside or outside an object. The pixel labeling problem is represented by a graph in which: (a) the nodes correspond to pixels (b) there exist weighted edges between each node and each pixel's 6 nearest neighboring nodes and (c) there exist weighted edges between each node and a high valued source (S) or to a low valued sink (T), which represent 'object' and 'background' states respectively. The edge weights between pixels are related to the intensity difference between the pixels. Once the graph has been established the graph-cut algorithm determines an optimal graph cut that has a minimum cost.

In our implementation, first all pixel intensities are scaled from the 16-bit original image to floating point values with a range from 0 to 1. Then for a particular pixel with a normalized intensity value I, the weight W_s between this pixel and the source and the weight W_t between this pixel and the sink is set as in equation (1)-(3). W_s indicates how strong a pixel is connected to source (brighter region in the image) and W_t indicates how strong it is connected to sink (darker region in the image). λ is the smoothing parameter that determines the ratio between W_s and I. The weight W_d between two connected pixels I_a and I_b is set as shown in equation (3), in which W_d and α determines the penalty of separating two pixels. If I_a equals I_b, the cost of cutting them is maximized. If I_a is very different from I_b, the cost of cutting them is relatively smaller.

$$W_s = \lambda * I \quad (1)$$

$$W_t = \lambda * (1-I) \quad (2)$$

$$W_d = e^{-\alpha*(I_a-I_b)^2} \quad (3)$$

The outcome of executing this graph-cut algorithm on a 3D optical CT image is shown in Figure 4. The top rows shows a central slice through the image and the lower row shows 3D visualizations of the outcome, which, in this case, corresponds to the nuclear region of the cell. The effect of changing the λ parameter for graph generation is shown. λ is a penalty term for separating a pixel from source or sink. A larger λ indicates a higher penalty. It is observed that as λ increases, the segmentation better captures the boundary details. However when λ reaches a certain value (for example 64), further increasing λ does not significantly influence the segmentation results.

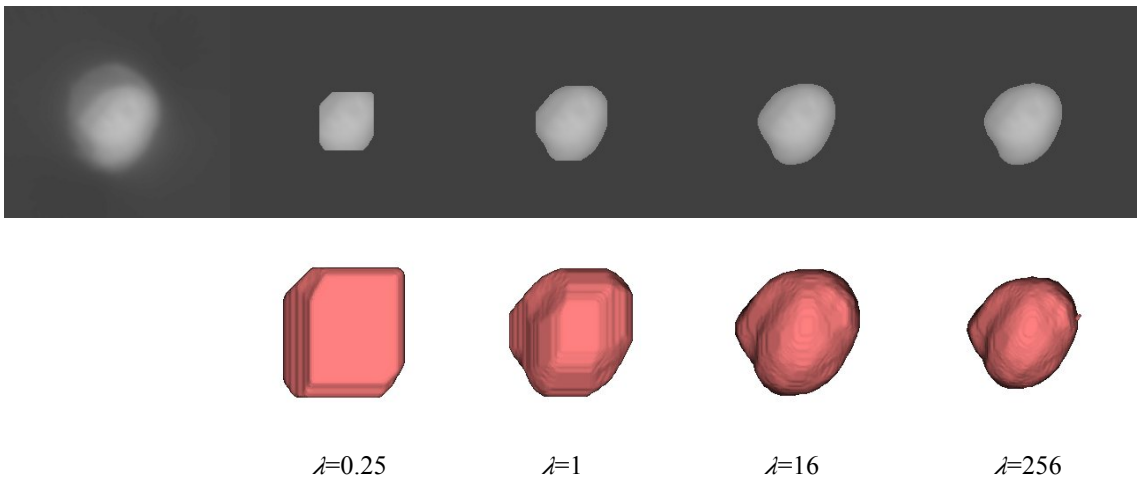

Figure 4. Different λ values and their respective segmentation result for the nucleus. Upper row: first image is a central 2D image slice and the others are the segmented nucleus with different λ. Lower row: their respective 3D visualization.

Downloaded From: http://proceedings.spiedigitallibrary.org/ on 08/10/2016 Terms of Use: http://spiedigitallibrary.org/ss/termsofuse.aspx

The cytoplasm part is less optically dense and has an intensity that is closer to the background. Therefore on the first application of the graph-cut the nucleus is segmented. A cell segmentation using the graph-cut method is shown for a central image slice through a cell in Figure 5. Figure 5(a) shows the image slice and Figure 5(b) shows the outcome of the first graph-cut segmentation. In order to segment the entire cell as an object, the intensity value of the nucleus is clipped so that it is similar to that of the cytoplasm as shown in Figure 5(c). When the graph-cut is applied to the clipped image the result is a segmentation between the whole cell (nucleus + cytoplasm) and the outside cell image background. The whole cell segmented region is shown in Figure 5(d). The following steps are used in the graph-cut segmentation algorithm:

(1) Apply the graph-cut algorithm to an intensity normalized 3D cell image. The segmented 'object' is considered nucleus and the 'background' is the cytoplasm plus the outside cell background.
(2) In order to better segment the cancer cells with intensity variations within the nucleus, a 3D convex hull algorithm is used on the segmented nucleus to ensure that it is a connected convex region (see discussion section).
(3) Clip the cell image with an intensity which is the mean intensity of the region adjacent to the segmented nucleus from step (2).
(4) Apply the graph-cut algorithm to the clipped image. The resulting segmented 'object' is considered as the entire cell.
(5) The cytoplasm is obtained by subtracting the nucleus part from the cell.

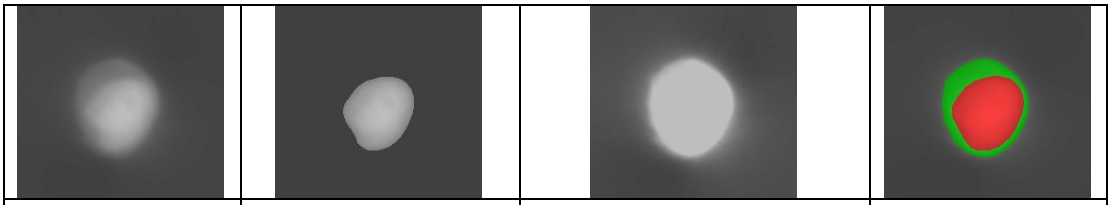

(a) Original Image | (b) Segmented Nucleus | (c) Intensity Transform Image | (d) Segmented Cell

Figure 5. Segmentation of the entire cell using graph-cut algorithm. From left to right: original image slice; segmented nucleus region using graph-cut; the intensity-transformed image based on segmented nucleus; the final segmentation result (nucleus in red and cytoplasm in green).

3. EXPERIMENTS AND RESULTS

To evaluate the two segmentation methods, a dataset of 248 3D optical-CT cell images was used in the experiment. It contains 5 different types of cells: 50 AF cells, 48 CO cells, 50 MA cells, 50 ME cells and 50 SQ cells. The images were randomly divided into a training set and a testing set. The testing set contained 200 images with 40 images per cell type while the other images were used for training. For all the images a manually marked boundary ground truth was available for both the nucleus and the cytoplasm. An example of the ground truth marking is shown by the yellow lines in Figure 6.

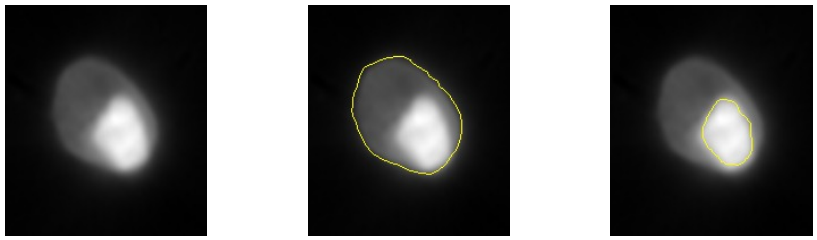

Figure 6. Manual marking example. From left to right: an axial image slice; manually marked cytoplasm boundary (in yellow) and manually marked nucleus boundary (in yellow).

Both 2D and 3D reference images were used in evaluation. For 2D evaluation, ground truth was obtained from 2D reference images having the nucleus and cytoplasm boundaries manually marked on a central axial slice as shown in Figure 6. For each cell, manual markings were only performed on one slice. Therefore, for 2D evaluation only the segmentation result on the corresponding slice was used.

Downloaded From: http://proceedings.spiedigitallibrary.org/ on 08/10/2016 Terms of Use: http://spiedigitallibrary.org/ss/termsofuse.aspx

For 3D evaluation, the 3D reference images were obtained by using a threshold that had a minimum Dice Similarity Coefficient (DSC) with respect to the manual 2D markings. For instance, a range of different threshold was used to separate nucleus region from the image. The threshold that resulted in the best segmentation, i.e. closest to the manual markings, was used for generating nucleus reference image. Similarly, another threshold was chosen for cytoplasm reference image. The resulting 3D reference image was compared with the 3D segmentation result.

The Dice Similarity Coefficient (DSC) is computed based on the 2D and 3D references. The DSC is defined as $2*tp/(2*tp+fp+fn)$, in which tp is the number of pixels detected in both manual and automatic segmentation, fp is the number of pixels detected only in automatic but not manual segmentation and fn is the number of pixels detected only in manual but not automatic segmentation. The average DSC between segmentation and reference images for each cell type is given in Table 1. For the 2D ground truth, the standard deviation of DSC using the graph cut with convex hull method was 0.14 for the nucleus and 0.20 for the cytoplasm. No visual assessment was performed in the evaluation stage.

Table 1. Two methods and their respective average DSC values compared to 2D and 3D ground truth. Method (1) and (2) are respectively gradient-based and graph cut with convex hull method. Ncl and Cyt denote nucleus and cytoplasm segmentation respectively.

DSC	AF		CO		MA		ME		SQ		All	
	(1)	(2)	(1)	(2)	(1)	(2)	(1)	(2)	(1)	(2)	(1)	(2)
2DNcl	0.61	0.89	0.80	0.89	0.70	0.80	0.79	0.84	0.72	0.90	0.72	0.86
2DCyt	0.40	0.68	0.48	0.64	0.71	0.68	0.65	0.82	0.33	0.77	0.51	0.72
3DNcl	0.61	0.83	0.78	0.87	0.71	0.77	0.77	0.82	0.70	0.88	0.71	0.83
3DCyt	0.43	0.68	0.47	0.66	0.73	0.70	0.65	0.86	0.26	0.82	0.51	0.75

4. DISCUSSION

A comparison of segmentation results using different methods is shown in Figure 7: the gradient based method, the graph-cut method without convex hull and the graph-cut method with convex hull. The graph-cut with convex hull method works very well for the cancer cells where nucleus intensities have a large variation. Figure 8 demonstrates the weakness of the gradient method. It performed well on images with rapid intensity changes and uniform intensity values in nucleus and cytoplasm (Figure 8 a and b). However, confusion may arise if the figure of merit has only one major peak (Figure 8 c) or more than two peaks (Figure 8 d). This is especially true for cancer cells due to the intensity variations within their nuclei.

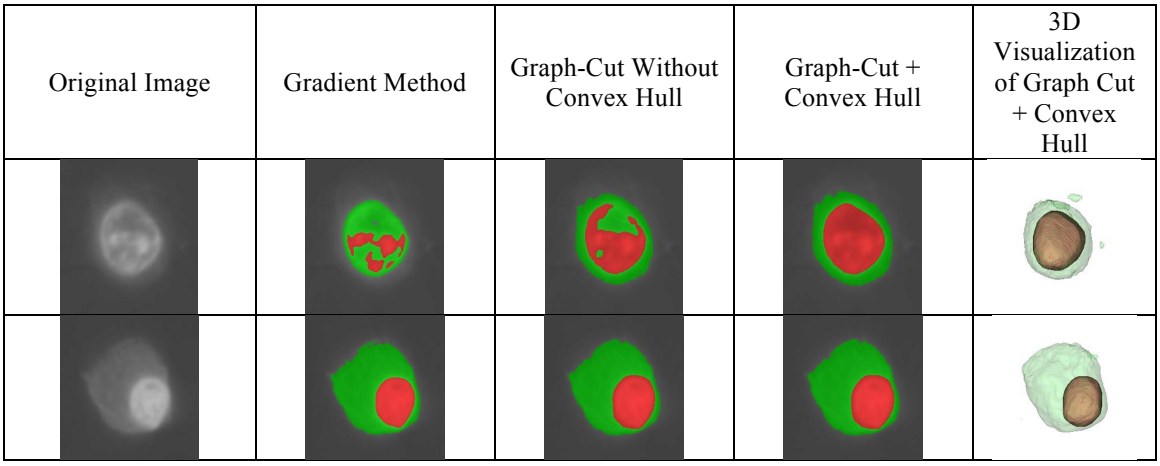

Figure 7. Comparison of different segmentation methods. From left to right: original images; segmentation using gradient, graph-cut without convex hull; graph-cut with convex hull and its 3D visualization. Red region denotes the segmented nucleus and green region denotes the segmented cytoplasm.

Downloaded From: http://proceedings.spiedigitallibrary.org/ on 08/10/2016 Terms of Use: http://spiedigitallibrary.org/ss/termsofuse.aspx

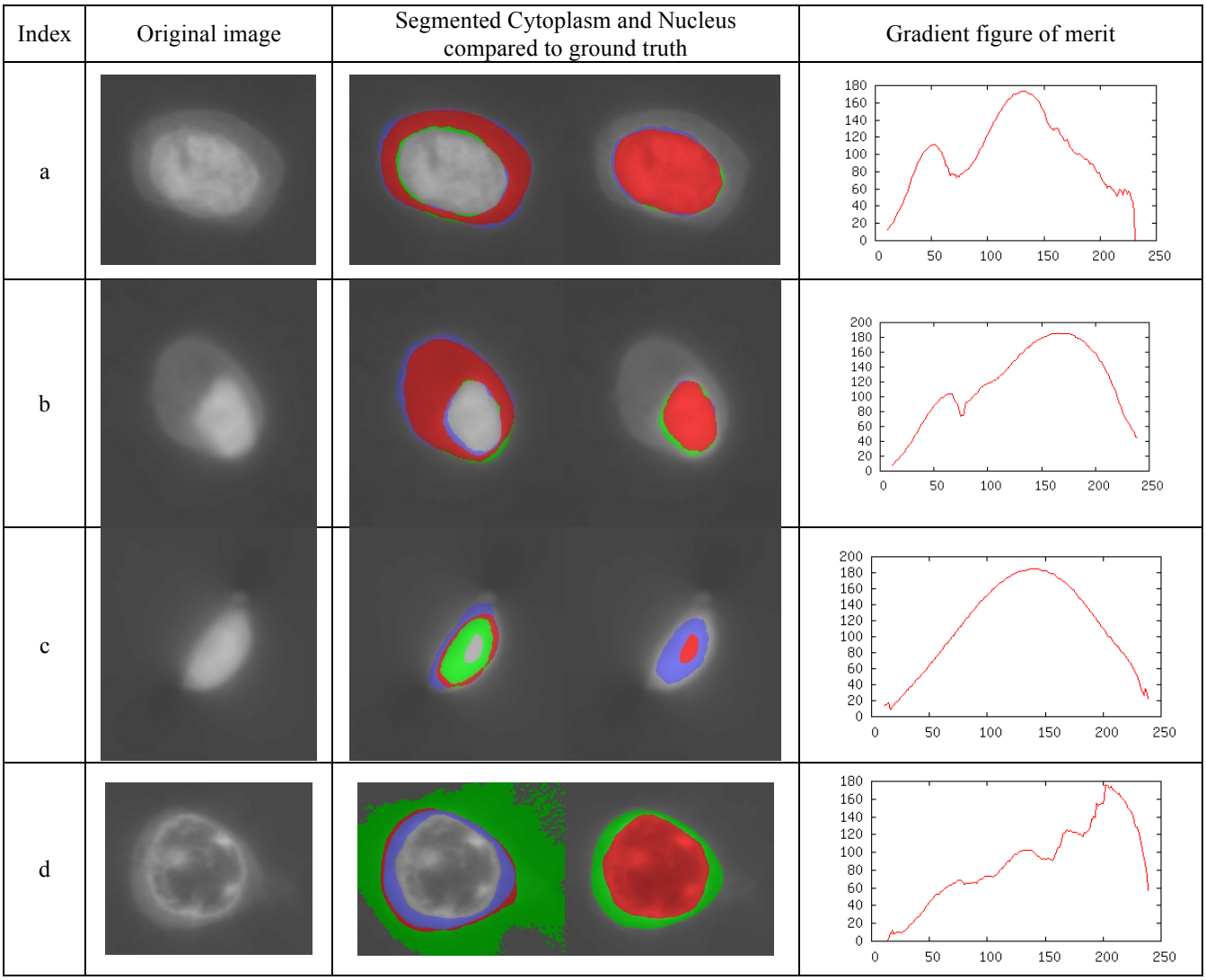

Figure 8. Examples of good and poor segmentations using gradient algorithm. From left to right: original image; segmented cytoplasm and nucleus against manual markings and the figure of merit curve. Red region exists in both automatic and manual segmentations, blue region only exists in manual segmentation and green region only exists in automatic segmentation.

The graph-cut with convex hull algorithm performed well, in general, on nucleus segmentation. However, for both methods, the DSC of cytoplasm was significantly lower than for the nucleus. This is mainly because cytoplasm usually has very similar intensity values as the background or does not have a well-defined shape. In such cases, manual markings did not appear to be as precise, which also resulted in the low DSC of cytoplasm segmentation. Figure 9 shows examples with poor segmentation of cytoplasm using the graph-cut with convex hull algorithm. Example 9 a, c, d, e and f all had good nucleus segmentation. However, the intensity values in their cytoplasm region are so similar to the background that it is very hard to determine the separation boundary. Example b shows a potential inaccuracy in manual markings. In most cases the dark region inside the cell would be considered as part of nucleus. However in this case the human marker determined that the dark region belongs to cytoplasm, thus causing the very low DSC in both nucleus and cytoplasm segmentation.

Downloaded From: http://proceedings.spiedigitallibrary.org/ on 08/10/2016 Terms of Use: http://spiedigitallibrary.org/ss/termsofuse.aspx

Index	Original image	Segmented Cyt and Ncl compared to ground truth	DSC
a.	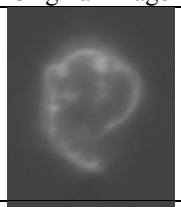	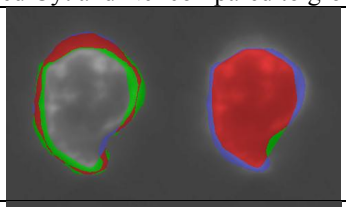	DSC_Cyt=0.62; DSC_Ncl=0.90;
b.	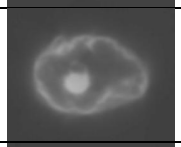	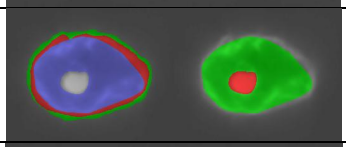	DSC_Cyt=0.30; DSC_Ncl=0.16;
c.		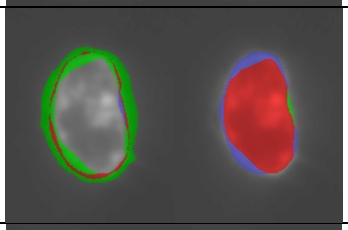	DSC_Cyt=0.26; DSC_Ncl=0.91;
d.	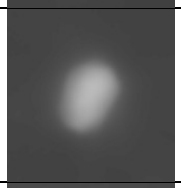	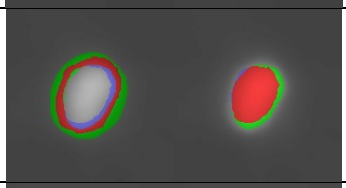	DSC_Cyt=0.57; DSC_Ncl=0.88;
e.	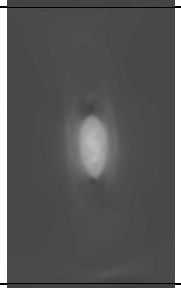	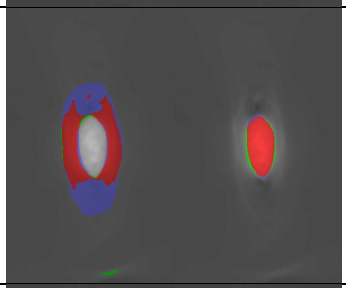	DSC_Cyt=0.66; DSC_Ncl=0.93;
f.	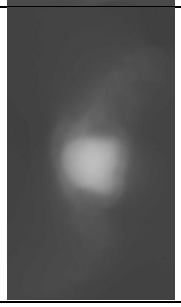	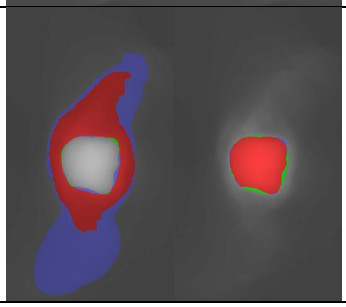	DSC_Cyt=0.61; DSC_Ncl=0.96;

Figure 9. Examples of poor cytoplasm segmentation (graph-cut with convex hull algorithm). From left to right: original image; segmented cytoplasm and nucleus against manual markings and their DSC. Red region exists in both automatic and manual segmentations, blue region only exists in manual segmentation and green region only exists in automatic segmentation.

5. CONCLUSION

The automated segmentation of single cell optical CT images is very challenging especially for cancer cells with high optical absorption variation. Two automated methods for segmentation have been considered; the first depends on a basic intensity model and determines a global threshold. The second method uses repeated applications of a graph-cut algorithm The graph-cut with convex hull method was able to perform accurate segmentation of nucleus and cytoplasm region in most images. Using an evaluation set of 200 3D cell images, this method achieved an average DSC of 86% and

Downloaded From: http://proceedings.spiedigitallibrary.org/ on 08/10/2016 Terms of Use: http://spiedigitallibrary.org/ss/termsofuse.aspx

72% in nucleus and cytoplasm segmentation respectively compared to the 2D reference images. The graph-cut method provides a robust algortihm for the segmentation of 3D optical CT single cell images.

ACKNOWLEDGEMENTS

This study was supported in part by the NSF grant, CBET-1014813 (PI-Reeves). The documented image data was provided by Michael Myer and VisionGate Inc.

REFERENCES

[1] Miao, Q., Reeves, A. P., Patten, F. W., and Seibel, E. J., "Multimodal 3D imaging of cells and tissue, bridging the gap between clinical and research microscopy." Annals of Biomedical Engineering. 40(2), 263-76 (2012).
[2] Fauver, M., and Seibel, E. J., "Three-dimensional imaging of single isolated cell nuclei using optical projection tomography." Opt. Express.13, 4210-4223 (2005).
[3] Reeves, A. P., Seibel, E. J., Meyer, M. G., Apanasovich, T., and Biancardi, A. M., "Nuclear cytoplasmic cell evaluation from 3D optical CT microscope images." SPIE Med. Imaging. 8315, 83153C (2012).
[4] Meyer, M. G , Fauver, M., Rahn, J. R., Neumann, T., Patten F. W., Seibel, E. J. and Nelson, A. C., "Automated cell analysis in 2D and 3D: a comparative study." Pattern Recognition. 42, 141-146 (2009).
[5] Boykov, Y., and Funka-Lea, G., "Graph cuts and efficient N-D image segmentation." IJCV. 70(2), 109-131 (2006).
[6] Deriche, R., “Using Canny’s criteria to derive a recursively implemented optimal edge detector.” IJCV. 1, 167-187 (1987).

Downloaded From: http://proceedings.spiedigitallibrary.org/ on 08/10/2016 Terms of Use: http://spiedigitallibrary.org/ss/termsofuse.aspx